Nonlinear estimation of respiratory-induced heart movements and its application in ECG/VCG signal processing

by

Leif Sörnmo[1], Magnus Åström[1], Elena Carro[1,2], Martin Stridh[1], Pablo Laguna[2]

[1] Signal Processing Group, Dept. of Applied Electronics,
Lund University, Lund, Sweden,
[2] Grupo de Tecnologías de las Comunicaciones, Departamento de Ingeniería
Electrónica y Comunicaciones, Centro Politécnico Superior,
Universidad de Zaragoza, Zaragoza, Spain.

Address for correspondence:
Dr. Leif Sörnmo
Signal Processing Group
Dept. of Applied Electronics
Lund University
Box 118,
S-221 00 Lund, Sweden

Telephone:	+46 46 222 90 23
Fax:	+46 46 222 47 18
e-mail:	`leif.sornmo@tde.lth.se`

April 26, 1999

1   Introduction

Electrocardiographic measurements from the body surface are often undesirably influenced by the presence of respiration-induced movements of the heart. Measures which quantify beat-to-beat variations in QRS morphology are particularly susceptible to this influence and special attention must therefore be given to this problem. The analysis of a vectorcardiographic (VCG) lead configuration has been found to reduce this problem. An important reason is that changes in the orientation of the electrical axis, caused by e.g. respiration, can to a certain degree be compensated for by VCG loop rotation. Such rotation can also improve the performance of serial VCG/ECG analysis in which two loops, recorded at different occasions, are compared in order to find pathological changes associated with e.g. myocardial infarction [1], [2].

In this chapter, a statistical signal model is described which compensates for heart movements by means of scaling and rotation in relation to a "reference" VCG loop [3]. Temporal loop misalignment is also parameterized within the model framework. The maximum likelihood (ML) estimator of the parameters describing these transformations is found to possess a nonlinear structure and involves e.g. singular value decomposition. The optimal parameter estimates can be determined without the need for iterative optimization techniques. Although the model initially assumes that two loops are to be aligned, the method can easily be extended to the case of multiple loop alignment.

The performance of the ML estimation method is assessed in the presence of noise and for different VCG loop morphologies. The results show that loop alignment can be done accurately at low to moderate noise levels. At high noise levels the estimation of rotation parameters breaks down in an abrupt manner. Furthermore, it is shown that the performance is strongly dependent on loop morphology; a planar loop is more difficult to align than is a nonplanar loop. The issue of measuring morphologic variability in combination with loop alignment has been investigated in [4]. Using an ECG simulation model based on propagation of action potentials in cardiac tissue, the ability of the method to separate morphologic variability of physiological origin from respiratory activity was studied. The results showed that the separation of these two activities can be done accurately up to moderate noise levels.

One application of the ML loop alignment is that of QRST complex cancellation for the analysis of atrial fibrillation in the surface ECG [5]. Again, shifts in the electrical axis of the heart cause the use of methods based on average beat subtraction to sometimes produce large QRST-related residuals. Using the loop alignment technique, residuals with a substantially lower amplitude were obtained and thereby the resulting residual ECG is much better suited for e.g. time/frequency analysis of atrial fibrillation. The new method for QRST complex cancellation is here briefly reviewed and an example illustrates the improved performance when compared to that of the average beat subtraction method.

2 Maximum likelihood VCG loop alignment

This section presents the essentials of the method for spatiotemporal alignment of VCG loops [3]. A statistical model is introduced in which a VCG loop is related to a reference loop by certain geometric transformations (Sec. 2.1). Maximum likelihood (ML) estimation is then investigated for finding those parameter values of the transformations which provide the optimal fit between the two loops (Sec. 2.2).

2.1 Model for respiratory-induced heart movements

The signal model is based on the assumption that an observed VCG loop of the QRS complex, $\mathbf{Y}$, derives from a reference loop, $\mathbf{Y}_R$, but has been altered through a series of transformations. The matrix $\mathbf{Y} = [\ \mathbf{y}_1\ \ \mathbf{y}_2\ \ \mathbf{y}_3\ ]$ contains column vectors $\mathbf{y}_l$ with N samples for the l:th VCG lead. The reference loop $\mathbf{Y}_R$ is $(N + 2\Delta)$-by-3 and includes 2Δ additional samples in order to allow for observations which constitute different consecutive subsets of N samples from $\mathbf{Y}_R$. The following transformations are considered:

Amplitude scaling   Loop expansion or contraction is modeled by the positive-valued, scalar parameter α and represents, in a simplistic way, the effect of variations in e.g. location of the heart or conductivity of the surrounding tissue. When considering the problem of QRST cancellation, see Sec. 5, the extension of α to a diagonal matrix which accounts for scaling in individual leads is found to improve the cancellation performance further.

Rotation   Rotational changes of the heart in relation to the electrode locations are accounted for by the orthonormal, 3-by-3 matrix $\mathbf{Q}$; orthonormality implies that $\mathbf{Q}^T\mathbf{Q} = \mathbf{I}$ where $\mathbf{I}$ is the identity matrix. Rotational changes are caused by, e.g., respiration or body position changes.

Time synchronization   Although $\mathbf{Y}$ is assumed to be reasonably well-synchronized in time to $\mathbf{Y}_R$ due to the preceding QRS detection, means for refining the time synchronization is introduced in the model by the shift matrix $\mathbf{J}_\tau$. Due to the larger size of $\mathbf{Y}_R$, the observed loop $\mathbf{Y}$ can result from any of the $(2\Delta + 1)$ possible positions in $\mathbf{Y}_R$. The shift matrix $\mathbf{J}_\tau$ is defined by the integer time shift τ,

$$\mathbf{J}_\tau\ =\ [\ \mathbf{0}_{\Delta+\tau}\ \ \mathbf{I}\ \ \mathbf{0}_{\Delta-\tau}\ ] \tag{1}$$

where $\tau = -\Delta, ..., \Delta$. The dimensions of the left and right zero matrices in (1) are equal to N-by-$(\Delta + \tau)$ and N-by-$(\Delta - \tau)$, respectively. One of the zero matrices vanishes when τ is $\pm\Delta$. The identity matrix $\mathbf{I}$ is N-by-N. By estimating the parameters which characterize these transformations, it will be possible to reduce the influence of extracardiac activities and thus to improve the alignment of $\mathbf{Y}$ to $\mathbf{Y}_R$.

The above scaling, rotation and time synchronization parameters are embraced by the following observation model

$$\mathbf{Y} = \alpha \mathbf{J}_\tau \mathbf{Y}_R \mathbf{Q} + \mathbf{W} \tag{2}$$

The transformed reference loop is assumed to be additively disturbed by white, Gaussian noise (represented by the N-by-3 matrix $\mathbf{W} = [\ \mathbf{w}_1 \quad \mathbf{w}_2 \quad \mathbf{w}_3 \ ]$). Furthermore, the noise is assumed to be uncorrelated from lead-to-lead and with identical variance, σ_w^2, in all leads. The noise probability density function is then given by

$$p_w(\mathbf{W}) = \prod_{l=1}^{3} p_w(\mathbf{w}_l) \quad = \quad \frac{1}{(2\pi)^{3N/2} \sigma_w^{3N}} \ e^{-\frac{1}{2\sigma_w^2} \sum_{l=1}^{3} \mathbf{w}_l \mathbf{w}_l^T} \tag{3}$$

$$= \quad \frac{1}{(2\pi)^{3N/2} \sigma_w^{3N}} \ e^{-\frac{1}{2\sigma_w^2} \mathrm{tr}(\mathbf{W}\mathbf{W}^T)} \tag{4}$$

where tr denotes the matrix trace.

2.2 Maximum likelihood estimation

The joint maximum likelihood (ML) estimator of the parameters α, $\mathbf{Q}$ and τ is derived by maximizing the log-likelihood function [6], i.e.

$$\frac{\partial}{\partial \alpha} \frac{\partial}{\partial \mathbf{Q}} \frac{\partial}{\partial \tau} \ln p_w(\mathbf{Y}|\alpha, \mathbf{Q}, \tau) = 0 \tag{5}$$

It can be shown that the calculation of (5) is equivalent to the minimization of the Frobenius norm ε^2 between $\mathbf{Y}$ and $\mathbf{Y}_R$ [3],

$$\varepsilon_{min}^2 = \min_{\alpha, \mathbf{Q}, \tau} \|\mathbf{Y} - \alpha \mathbf{J}_\tau \mathbf{Y}_R \mathbf{Q}\|_F^2 \tag{6}$$

The Frobenius norm for an m-by-n matrix $\mathbf{X}$ is defined by

$$\|\mathbf{X}\|_F^2 = \mathrm{tr}(\mathbf{X}\mathbf{X}^T) = \sum_{i=1}^{m} \sum_{j=1}^{n} |x_{ij}|^2 \tag{7}$$

The minimization in (6) is performed by first finding closed-form expressions for the estimates α and $\mathbf{Q}$ under the assumption that τ is fixed. The optimal estimates of α, $\mathbf{Q}$ and τ are then determined by evaluating the error ε^2 for all values of τ in the interval $[-\Delta, \Delta]$.

The estimate of $\mathbf{Q}$ is obtained by first rewriting the error in (6) such that

$$\varepsilon^2 = \mathrm{tr}(\mathbf{Y}\mathbf{Y}^T) + \alpha^2 \ \mathrm{tr}(\mathbf{J}_\tau \mathbf{Y}_R \mathbf{Y}_R^T \mathbf{J}_\tau^T) - 2\alpha \ \mathrm{tr}(\mathbf{Y}_R^T \mathbf{J}_\tau^T \mathbf{Y}\mathbf{Q}^T) \tag{8}$$

and then noting that (8) is minimized by choosing $\mathbf{Q}$ such that the last term $tr(\mathbf{J}_\tau^T \mathbf{Y}_R^T \mathbf{Q}^T \mathbf{Y})$ is maximized. The key step in finding the optimal $\mathbf{Q}$ is to use the singular value decomposition (SVD) [7]. In general, the SVD provides a

4

decomposition of the M-by-N matrix $\mathbf{Z}$ into the orthonormal matrices $\mathbf{U}$ (M-by-M) and $\mathbf{V}$ (N-by-N) and the diagonal matrix $\mathbf{\Sigma}$ with the singular values ($\mathbf{\Sigma} = \mathrm{diag}(\sigma_1, \ldots, \sigma_l, 0, \ldots, 0)$, $l = \min(M, N)$),

$$\mathbf{Z} = \mathbf{U}\mathbf{\Sigma}\mathbf{V}^T \tag{9}$$

In particular, by defining the 3-by-3 matrix $\mathbf{Z}$ such that

$$\mathbf{Z}_\tau = \mathbf{Y}_R^T \mathbf{J}_\tau^T \mathbf{Y} \tag{10}$$

the last term on the right hand side of (8) can be rearranged and expressed as

$$\mathrm{tr}(\mathbf{Y}_R^T \mathbf{J}_\tau^T \mathbf{Y}\mathbf{Q}^T) = \mathrm{tr}(\mathbf{Z}_\tau \mathbf{Q}^T) \tag{11}$$

By choosing $\mathbf{Q}$ such that $\mathbf{U}\mathbf{V}^T\mathbf{Q}^T = \mathbf{I}$, the expression in (11) is maximized and the resulting ML estimate is given by

$$\hat{\mathbf{Q}}_\tau = \mathbf{U}\mathbf{V}^T \tag{12}$$

The index τ has been attached in (12) since this estimate is optimal for only one particular value of τ.

The estimate of α can be calculated when $\hat{\mathbf{Q}}_\tau$ is available,

$$\hat{\alpha}_\tau = \frac{\mathrm{tr}(\mathbf{Y}_R^T \mathbf{J}_\tau^T \mathbf{Y}\hat{\mathbf{Q}}_\tau^T)}{\mathrm{tr}(\mathbf{J}_\tau \mathbf{Y}_R \mathbf{Y}_R^T \mathbf{J}_\tau^T)} \tag{13}$$

The discrete-valued time synchronization parameter τ is estimated by means of a grid search for the allowed set of values,

$$\hat{\tau} = \arg\min_\tau \|\mathbf{Y} - \hat{\alpha}_\tau \mathbf{J}_\tau \mathbf{Y}_R \hat{\mathbf{Q}}_\tau\|_F^2 \tag{14}$$

Finally, the estimate $\hat{\tau}$ determines which of the estimates in the set of estimates $\hat{\alpha}_\tau$ and $\hat{\mathbf{Q}}_\tau$ that should be selected. It is noted that the above estimation procedure always yields the optimal estimates since τ belongs to a finite set of values; the continuous-valued estimates $\hat{\alpha}$ and $\hat{\mathbf{Q}}$ are obtained conditioned on τ. Furthermore, it should be noted that the resulting ML estimator, as defined by (12), (13) and (14), exhibit a nonlinear structure although the observation model in (2) has a linear characteristic.

Application of the above ML estimation procedure requires that a reference loop $\mathbf{Y}_R$ has been first defined. In the simplest case of aligning two loops, $\mathbf{Y}_R$ can be taken as any of the two available loops. When several loops $\{\mathbf{Y}_i\}_{i=1}^M$ are to be aligned, implying that the observation model is extended to $\mathbf{Y}_i = \alpha_i \mathbf{J}_{\tau,i} \mathbf{Y}_R \mathbf{Q}_i + \mathbf{W}_i$ for $i = 1, ..., M$, a variety of definitions of $\mathbf{Y}_R$ are possible.

The samples of the matrices $\mathbf{Y}$ and $\mathbf{Y}_R$ are assumed to be appropriately centered around the QRS complex. The 2Δ samples are equally divided into samples being prepended and appended to the QRS centered interval, respectively. It should be noted that the noise variance σ_w^2 does not enter the ML estimation procedure and thus no estimate is required of this parameter.

5

Before demonstrating the effect of loop alignment, it should be pointed out that $\hat{\mathbf{Q}}$ can be used for retrieving information related to respiration. Such respiratory-related patterns are made more obvious by decomposing $\hat{\mathbf{Q}}$ into a product of three planar rotation matrices, where the angles φ_X, φ_Y and φ_Z define the rotation around each lead axis. These angles can be estimated by [3],

$$
\begin{aligned}
\hat{\varphi}_Y &= \arcsin(\hat{q}_{13}) \\
\hat{\varphi}_X &= \arcsin(\frac{\hat{q}_{12}}{\cos\hat{\varphi}_Y}) \\
\hat{\varphi}_Z &= \arcsin(\frac{\hat{q}_{23}}{\cos\hat{\varphi}_Y})
\end{aligned}
\qquad (15)
$$

where the estimate $\hat{q}_{kl}$ denotes the (k,l):th element of $\hat{\mathbf{Q}}$. The idea of studying angular changes in axis orientation as a basis for estimating the respiratory rate was suggested in the mid 80's, see e.g. [8], [9]; in those studies, however, the angles were estimated with techniques different from that presented here.

3 Loop alignment and morphologic variability

The above ML loop alignment method can, as pointed out in Sec. 1, compensate for certain limitations associated with the analysis of subtle beat-to-beat variations in QRS morphology. This type of analysis has recently received clinical attention due to its potential value for diagnosing myocardial ischemia and acute infarction, see e.g. [10], [11], [12]. It has been hypothesized that subtle morphologic variations may reflect e.g. islets of ischemic tissue or variations in myocardial contraction patterns. Straightforward computation of the standard deviation for a time-aligned ensemble of beats has been suggested as a means for describing such morphologic beat-to-beat variability [13]. Unfortunately, few techniques have been presented in the literature which aim at reducing the undesirable influence of respiration. This is somewhat surprising since it is well-known that the electrical axis can vary as much as $10°$ in the transversal plane during inspiration [14].

The examples presented below illustrate the effect of ML loop alignment in terms of morphologic beat-to-beat variability. In each example, fifty consecutive sinus beats were selected from a high-resolution ECG recording using an orthogonal lead configuration (X, Y and Z). The sampling rate was equal to 1000 Hz and the amplitude resolution was $0.6 \ \mu V$. The recordings were selected from a database of subjects with previous myocardial infarction and/or episodes of sustained ventricular tachycardia. Noisy and aberrant beats were excluded from further analysis. The reference beat was simply selected as the first one out of the fifty beats. Finally, the ensemble standard deviation was employed as a measure of morphologic variability and was computed both before and after loop alignment.

The effect of loop alignment is demonstrated by the example in Fig. 1 (a)–(c); the corresponding parameter estimates of $\alpha, \varphi_X, \varphi_Y, \varphi_Z, \varepsilon$ and ε_{min} are shown in Fig. 1 (d)–(f) as functions of time. It is obvious from Fig. 1 (e)–(f) that reduction in variability is related to scaling as well as to rotation of the loops. For ease

6

of interpretation, the results in Fig. 1 (a)–(c) are presented for individual leads although the alignment is an inherently spatiotemporal process.

Oscillatory patterns found in the error norm are likely to be related to respiratory activity. Such oscillations can be discerned in Fig. 1 (d) both before and after loop alignment although the oscillations are less pronounced after alignment. However, in certain cases the model parameters are able to account very well for the oscillatory component in ε_{min}, see Fig. 2 (d). It is noted that the variability in lead X is essentially removed after loop alignment while the reduction in the other two leads is less dramatic (cf. the variation in the angle φ_X).

4 Sensitivity of loop alignment to noise

Loop alignment may be of interest to use in noisy situations for the purpose of e.g. QRST complex cancellation (see Sec. 5) or for the analysis of data acquired during exercise. In this section, the noise properties of the rotation matrix estimate are studied in terms of accuracy of estimated rotation angles. Based on these results, the concept of a *breakdown noise level* is introduced to describe an essential characteristic of the angle estimates. This concept is then used to investigate the effect of different loop morphologies in the alignment process [4].

4.1 Parameter estimation

A "signal–plus–noise" simulation model similar to that in (2) is here adopted in order to get an appreciation of how noise influences alignment performance. A VCG loop was selected from a healthy individual as the signal part of the model after reduction of the inherent noise level by conventional signal averaging (the loop was included in the database considered in Sec. 4.2). The loop is then subjected to rotation on a sample-to-sample basis in order to account for respiratory-induced noise, i.e. the matrix $\mathbf{Q}$ is a function of time k. The resulting simulation model is defined by

$$
\begin{bmatrix} z_1(k) \\ z_2(k) \\ z_3(k) \end{bmatrix} = \mathbf{Q}(k) \begin{bmatrix} y_1(k) \\ y_2(k) \\ y_3(k) \end{bmatrix} + \begin{bmatrix} v_1(k) \\ v_2(k) \\ v_3(k) \end{bmatrix} \tag{16}
$$

where $(y_1(k), y_2(k), y_3(k))$ constitute the original VCG loop at sample k. The additive noise $v_i(k)$ is assumed to be white Gaussian with variance equal to σ_v^2 and with no interlead correlation.

The matrix $\mathbf{Q}(k)$ in (16) is assigned a specific structure by the angles which characterize the three planar rotation matrices of $\mathbf{Q}(k)$. It is assumed that the angular variation in each lead is proportional to the amount of air in the lungs during a respiratory cycle. A simplistic way to model this property is to use the product of two sigmoidal functions to describe the inspiratory and expiratory phases, respectively. The angular variation in lead X is defined by

$$
\varphi_X(k) = \eta_X \left(\frac{1}{1 + e^{\lambda_{in}(k - \kappa_{in})}} \right) \left(\frac{1}{1 + e^{\lambda_{ex}(k - \kappa_{ex})}} \right) \tag{17}
$$

7
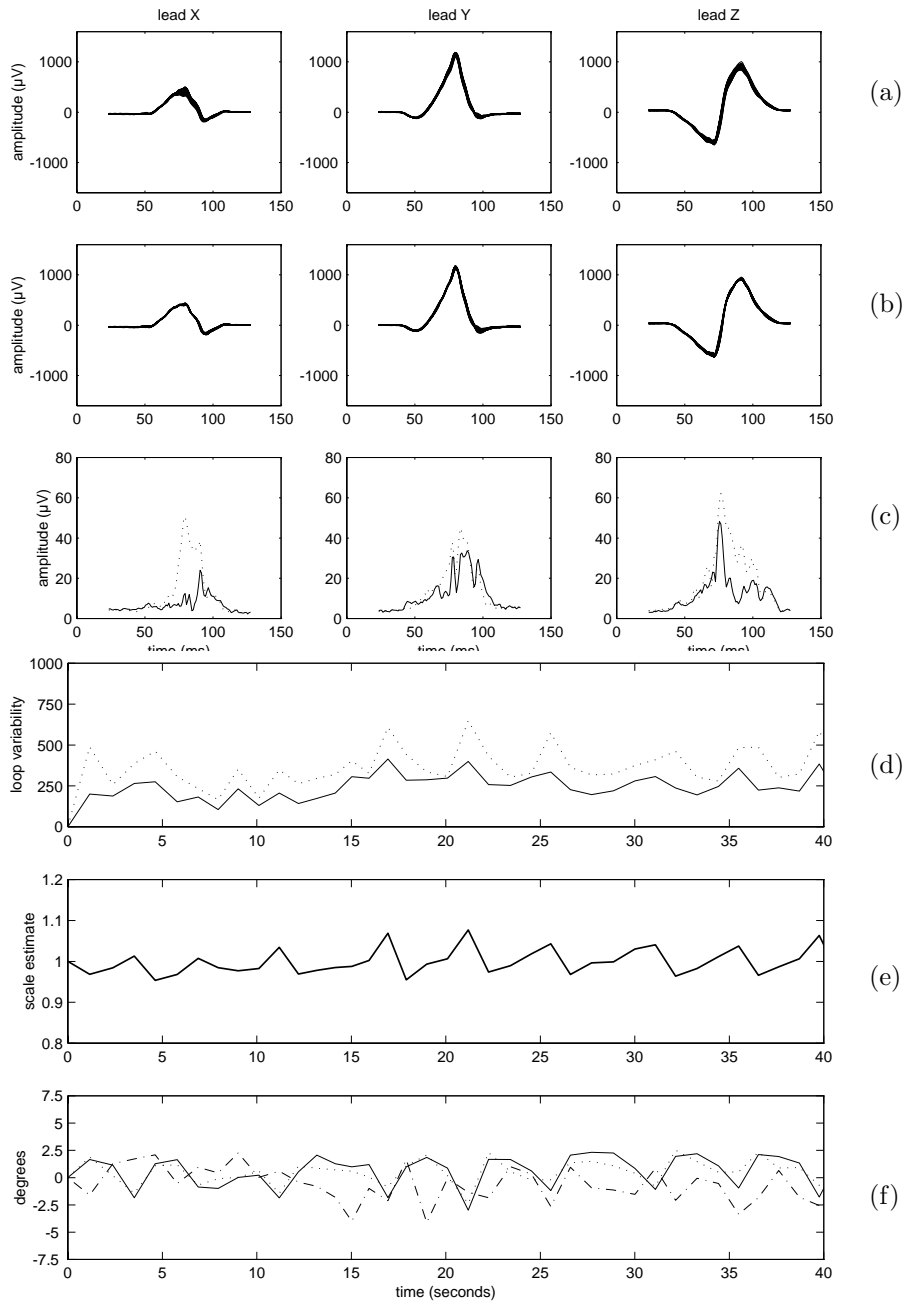
Figure 1: An example of fifty superimposed beats (a) before loop alignment, (b) after alignment, and (c) the corresponding ensemble standard deviation (dotted and solid line correspond to (a) and (b), respectively), (d) spatial variability before (dotted line) and after loop alignment (ε_{min} in (6); solid line), (e) the scaling estimate $\hat{\alpha}$ and (f) the angle estimates $\hat{\varphi}_X$, $\hat{\varphi}_Y$ and $\hat{\varphi}_Z$ (solid, dotted and dashed/dotted line, respectively).

8
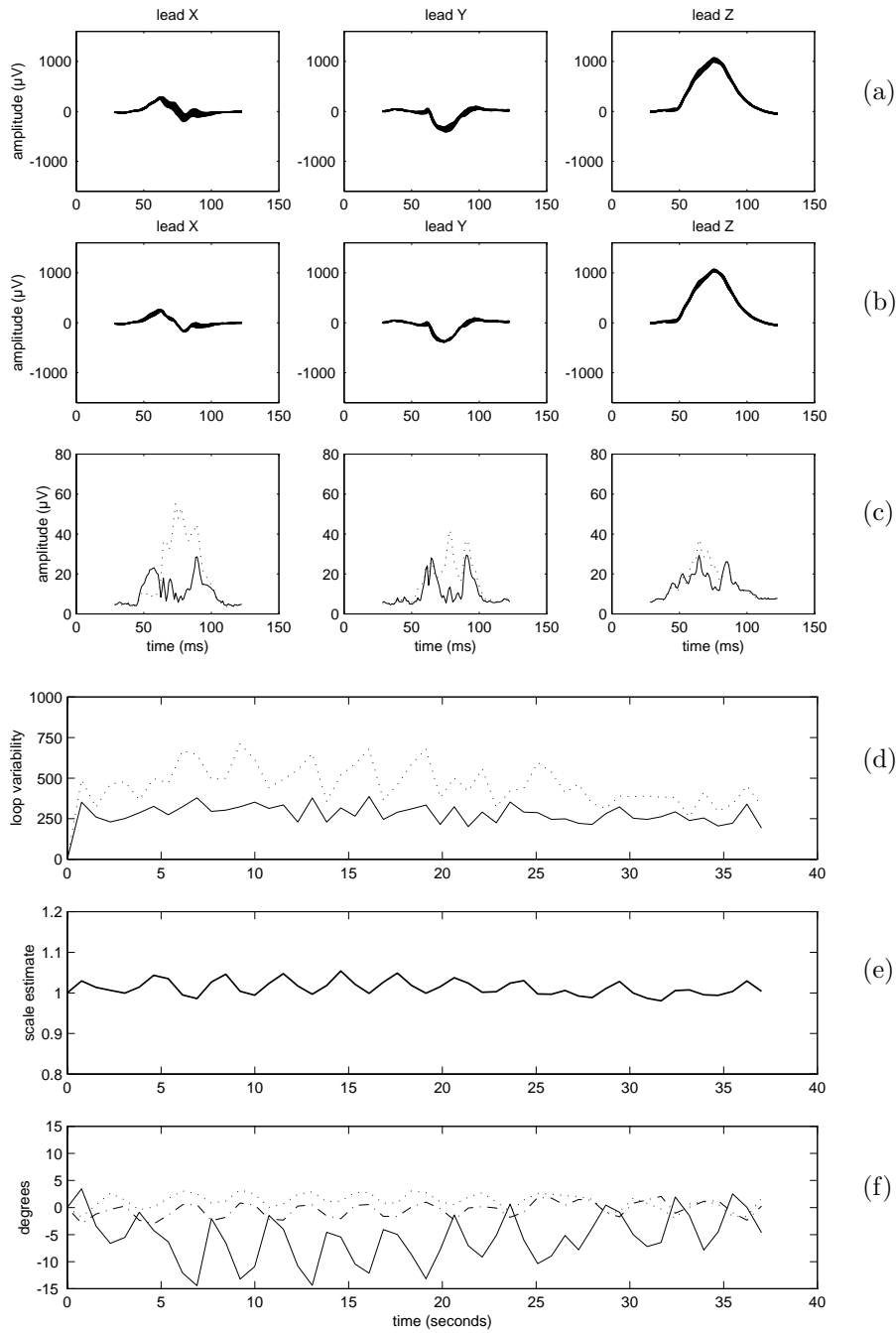
Figure 2: An example with large morphologic variability in which the ML loop alignment dramatically reduces the oscillatory component in ε. Again, fifty superimposed beats are shown (a) before loop alignment, (b) after alignment, and (c) the corresponding ensemble standard deviation (dotted and solid line correspond to (a) and (b), respectively), (d) spatial variability before (dotted line) and after loop alignment (ε_{min} in (6); solid line), (e) the scaling estimate $\hat{\alpha}$ and (f) the angle estimates $\hat{\varphi}_X$, $\hat{\varphi}_Y$ and $\hat{\varphi}_Z$ (solid, dotted and dashed/dotted line, respectively).

9
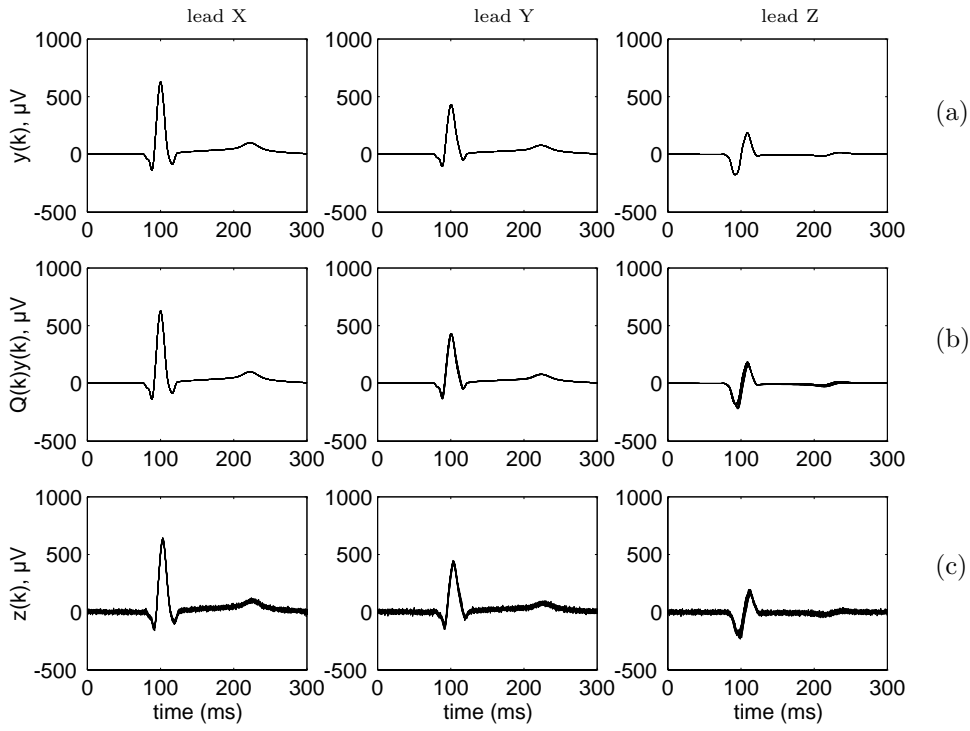
Figure 3: An example of fifty superimposed beats at various stages in the simulation model. (a) without added noise, (b) after transformation with **Q** and (c) with noise added ($\sigma_v = 10\mu$V).

where the duration of inspiration and expiration are determined by λ_{in} and λ_{ex}, respectively, and the time delays of the sigmoidal functions by κ_{in} and κ_{ex}. The parameter η_X is an amplitude factor. The angular variation in leads Y and Z are defined in an analogous manner.

Signals at various stages in the simulation model in (16) are shown in Fig. 3 and the corresponding rotation pattern is shown in Fig. 4 (a). In this example, rotation is only introduced around the X axis and therefore the morphology of the beats in Fig. 3 (b) changes only in leads Y and Z. The rotation angles were estimated from the noisy signal using (15) and are presented in Fig. 4 (b).

A comparison of the original angles and the estimated ones must account for that the original angles are time-varying while only one angle estimate is obtained for the entire QRS complex. Therefore, the average of $\varphi(k)$ during the QRS complex was used as the reference value. The root mean square error measure for the angle estimates is then given by

$$\delta = \sqrt{\frac{1}{B}\sum_{i=1}^{B}(\hat{\varphi}_i - \bar{\varphi}_i)^2} \tag{18}$$

where B denotes the number of beats, $\hat{\varphi}_i$ and $\bar{\varphi}_i$ denote the angle estimate and the corresponding average reference value, respectively, of the i:th beat. It should be noted that the error present in δ due to the once-per-beat estimate of the loop alignment method is negligible for realistic choices of respiratory rates.

Figure 4 (c) presents the error measure δ for each of the X, Y and Z leads as a function of the noise level σ_v. An interesting behavior can be observed in lead Z where a distinct noise level exists (approximately 18 μV) above which the performance rapidly deteriorates and large estimation error results. Since this threshold behavior was observed in all other VCG recordings analyzed in this study (cf. the results in Sec. 4.2), it seems well motivated to use the concept of breakdown noise level. In the present example, the behavior can also be observed in the other leads although the decrease in performance is not as drastic as in lead Z. The original angle pattern and the corresponding estimated pattern in Fig. 4 (a)–(b) exemplifies the outlier angle estimates which occur at three points in time.

4.2 Noise and loop morphology

The results in the previous section suggest that it may be of interest to investigate the relation between breakdown noise level and loop morphology. In order to investigate this aspect a database was used with 34 non-selected individuals being referred for myocardial scintigraphy [15]. These individuals had no signs of ischemia or infarction. The ECG signals were recorded during rest for five minutes using a standard 12 lead configuration. The VCG signals were then synthesized by means of linear combination of the 12 leads using the inverse Dower weighting matrix [16].

In order to characterize loop morphology, an over-all measure was considered which reflects the planarity of a VCG loop. The measure is defined as the ratio
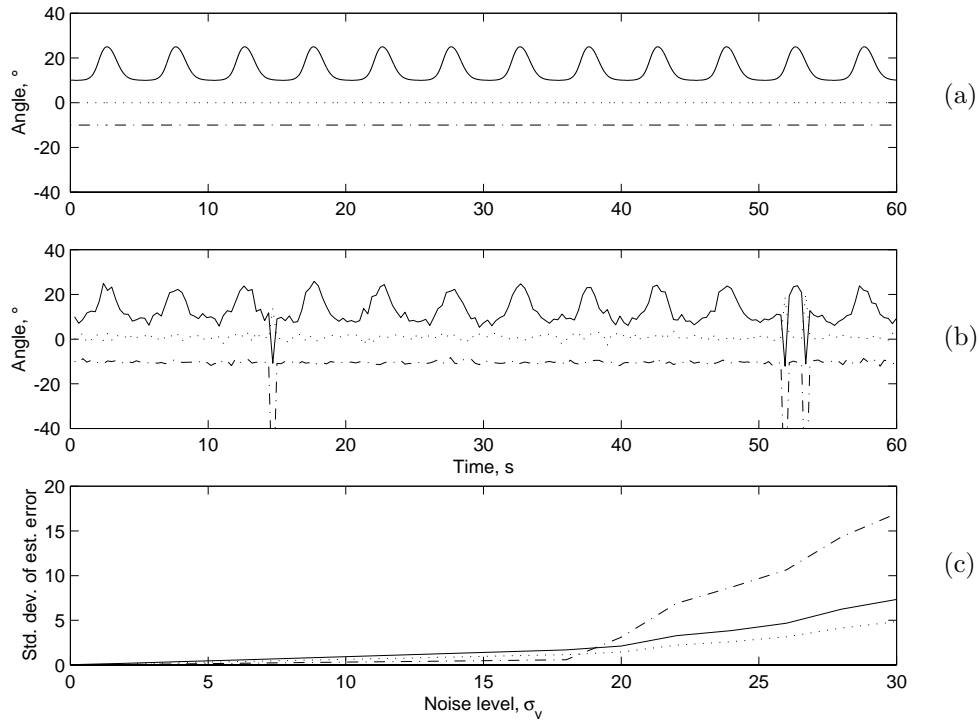
Figure 4: Example of (a) angular variation pattern and (b) the corresponding estimates obtained from a signal disturbed by noise with variance $\sigma_v^2 = 10\mu$V. The angle patterns are plotted with a five degree displacement for each lead in order to improve legibility. (c) The angle estimation error δ as a function of noise variance.

between the minimum and the maximum singular values of the loop matrix $\mathbf{Y}$, i.e.

$$\rho = \frac{\sigma_{min}}{\sigma_{max}} \qquad (19)$$

The limiting values of ρ are 0 (a loop which is perfectly planar) and 1 (a loop which extends equally into all three dimensions).

The breakdown noise level, denoted $\tilde{\sigma}_v$, is defined as that noise level σ_v which causes angle estimation errors in any lead to exceed a certain threshold χ. The choice of χ was based on the observation that the estimation error is small below a certain noise level while then rapidly increasing to a considerably larger error value. By setting χ equal to $\pi/10$, proper identification of the noise level at which angle estimates became anomalous was achieved.

Figure 5 shows that the accuracy of loop alignment with regard to noise level is strongly dependent on loop planarity; the breakdown noise level $\tilde{\sigma}_v$ actually ranges from 5 to 70 μV. This result suggests that an essentially linear relationship exists between ρ and $\tilde{\sigma}_v$. It can be concluded that aligning planar loops is much more vulnerable to noise than is the alignment of a loop extending into all three dimensions.

It is well-known that normal individuals in general have VCG loops which are more planar than those from patients with e.g. myocardial infarction. For example, myocardial damage is often associated with loops which include abnormal transitions ("bites") or sharp edges and therefore decreases planarity [17]. Such differences in loop characteristics may thus imply that alignment, in general, is more robust in infarct patients than in normal individuals.

5   Spatiotemporal alignment and QRST cancellation

The characterization of atrial fibrillation (AF) using the surface ECG is facilitated by the derivation of a signal in which the ventricular activity has been first canceled. Since the atrial and the ventricular activities overlap spectrally, techniques based on linear filtering are less suitable. Instead, an average beat subtraction (ABS) method has been suggested which makes use of the fact that AF is uncoupled to ventricular activity. Subtraction of the average beat, which thus reflects the ventricular activity, produces a residual ECG containing essentially the fibrillation waveforms, i.e. the f waves [18], [19], [20].

The performance of the ABS method relies on the assumption that the average beat can represent each individual beat accurately. However, as pointed out earlier in this chapter, the QRS complexes are often subject to beat-to-beat changes in morphology which, due to the single lead nature of the ABS method, can cause large QRS-related residuals. The present loop alignment technique is further developed below in order to improve the cancellation of QRST complexes [5].
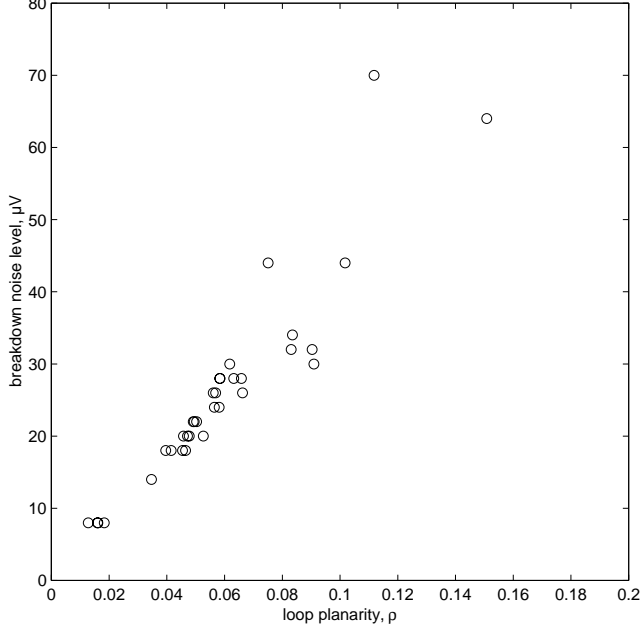
Figure 5: The relationship between loop planarity and breakdown noise level.

5.1 Signal model with lead-dependent amplitude scaling

The QRST cancellation problem is based on a model similar to that in (2) but with the amplitude scaling factor α being replaced by a diagonal matrix $\mathbf{D}$ which accounts for scaling in individual leads, i.e.

$$\mathbf{Y} = \mathbf{J}_\tau \mathbf{Y}_R \mathbf{D} \mathbf{Q} + \mathbf{F} \tag{20}$$

The average beat ("the reference beat") is denoted with $\mathbf{Y}_R$ and the fibrillation activity with $\mathbf{F}$.

Again, the objective is to find those model parameter values which provide the best fit of the model to the observed signal. An estimate of the fibrillation signal $\mathbf{F}$ could be obtained by subtracting a scaled, rotated and time shifted version of $\mathbf{Y}_R$ from $\mathbf{Y}$,

$$\mathbf{F} = \mathbf{Y} - \mathbf{J}_{\hat{\tau}} \mathbf{Y}_R \hat{\mathbf{D}} \hat{\mathbf{Q}} \tag{21}$$

The Frobenius norm to be minimized is, in an expanded format, equal to

$$\epsilon^2 = \mathrm{tr}(\mathbf{Y}\mathbf{Y}^T) + \mathrm{tr}(\mathbf{J}_\tau \mathbf{Y}_R \mathbf{D}\mathbf{D}^T \mathbf{Y}_R^T \mathbf{J}_\tau^T) - 2\mathrm{tr}(\mathbf{D}^T \mathbf{Y}_R^T \mathbf{J}_\tau^T \mathbf{Y} \mathbf{Q}^T) \tag{22}$$

Unfortunately, the minimization with respect to rotation and amplitude scaling can no longer be performed independently as was the case in Sec. 2.2. Since the exact solution is difficult to find, an alternating iterative approach is used in which the error in (22) for a fixed $\mathbf{D}$ is minimized with respect to $\mathbf{Q}$ by maximizing the

14

last term. In order to find $\hat{\mathbf{Q}}$, the SVD is again employed but now operating on a different matrix,

$$\mathbf{Z} = \mathbf{D}^T\mathbf{Y}_R^T\mathbf{J}_\tau^T\mathbf{Z} = \mathbf{U}\mathbf{\Sigma}\mathbf{V}^T \tag{23}$$

As in Sec. 2.2, the estimate of $\mathbf{Q}$ is given by the product of the matrices $\mathbf{U}$ and $\mathbf{V}^T$ containing the left and right singular vectors, respectively, cf. the expression in (12).

When an estimate of $\mathbf{Q}$ is available, (22) can be written as

$$\epsilon^2 = tr(\mathbf{Y}\mathbf{Q}^{-1} - \mathbf{J}_\tau\mathbf{Y}_R\mathbf{D})\mathbf{Q}\mathbf{Q}^T(\mathbf{Y}\mathbf{Q}^{-1} - \mathbf{J}_\tau\mathbf{Y}_R\mathbf{D})^T \tag{24}$$

where the introduction of $\mathbf{Y}_2 = \mathbf{Y}\mathbf{Q}^{-1}$ yields

$$\epsilon^2 = \|\mathbf{Y}_2 - \mathbf{J}_\tau\mathbf{Y}_R\mathbf{D}\|_F^2 \tag{25}$$

Equation (25) can now be rearranged as

$$\epsilon^2 = \mathrm{tr}(\mathbf{Y}_2\mathbf{Y}_2^T) + \mathrm{tr}(\mathbf{D}\mathbf{D}^T\mathbf{Y}_R^T\mathbf{J}_\tau^T\mathbf{J}_\tau\mathbf{Y}_R) - 2\mathrm{tr}(\mathbf{D}^T\mathbf{Y}_R^T\mathbf{J}_\tau^T\mathbf{Y}_2) \tag{26}$$

which is minimized by setting the derivative with regard to $\mathbf{D}$ to zero, i.e.

$$\frac{d\epsilon^2}{d\mathbf{D}} = 2\mathbf{D}\mathbf{Y}_R^T\mathbf{J}_\tau^T\mathbf{J}_\tau\mathbf{Y}_R - 2\mathbf{Y}_R^T\mathbf{J}_\tau^T\mathbf{Y}_2 = 0 \tag{27}$$

The constraint of $\mathbf{D}$ as a diagonal matrix implies that (27) should be evaluated for individual leads. The diagonal entries in $\mathbf{D}$ can therefore be estimated by

$$\hat{d}_l = ([\mathbf{J}_\tau\mathbf{Y}_R]_l^T[\mathbf{J}_\tau\mathbf{Y}_R]_l)^{-1}([\mathbf{J}_\tau\mathbf{Y}_R]_l^T[\mathbf{Y}_2]_l) \tag{28}$$

For a given $\mathbf{Q}$, the above expression estimates the scale factors of the average beat before rotation. Based on the new scaling factors an improved rotation matrix can then be estimated.

Typically, a solution is desired which implies small rotation/scaling, i.e. $\mathbf{Q}$ and $\mathbf{D}$ are close to $\mathbf{I}$. The alternating, iterative procedure for finding the parameter estimates is therefore initialized by $\mathbf{D}_0 = \mathbf{I}$. The rotation at step k, $\mathbf{Q}_k$, is then calculated based on $\mathbf{D}_{k-1}$. Since

$$\|\mathbf{Y} - \mathbf{J}_\tau\mathbf{Y}_R\mathbf{D}_{k-1}\mathbf{Q}_k\|_F^2 \leq \|\mathbf{Y} - \mathbf{J}_\tau\mathbf{Y}_R\mathbf{D}_{k-1}\mathbf{Q}_{k-1}\|_F^2 \tag{29}$$

the error will be less or equal to that in the previous step. When $\mathbf{Q}_k$ is known, $\mathbf{D}_k$ can be calculated. Accordingly,

$$\|\mathbf{Y} - \mathbf{J}_\tau\mathbf{Y}_R\mathbf{D}_k\mathbf{Q}_k\|_F^2 \leq \|\mathbf{Y} - \mathbf{J}_\tau\mathbf{Y}_R\mathbf{D}_{k-1}\mathbf{Q}_k\|_F^2 \tag{30}$$

This procedure is then repeated until convergence is achieved. The algorithm will converge since the minimization with regard to both $\mathbf{Q}$ and $\mathbf{D}$ for each step according to (29) and (30) will improve the fit in terms of ϵ^2 [21].

One difficulty in performing the above alignment is that the presence of AF influences the signal amplitude during the QRS interval. It is therefore desirable
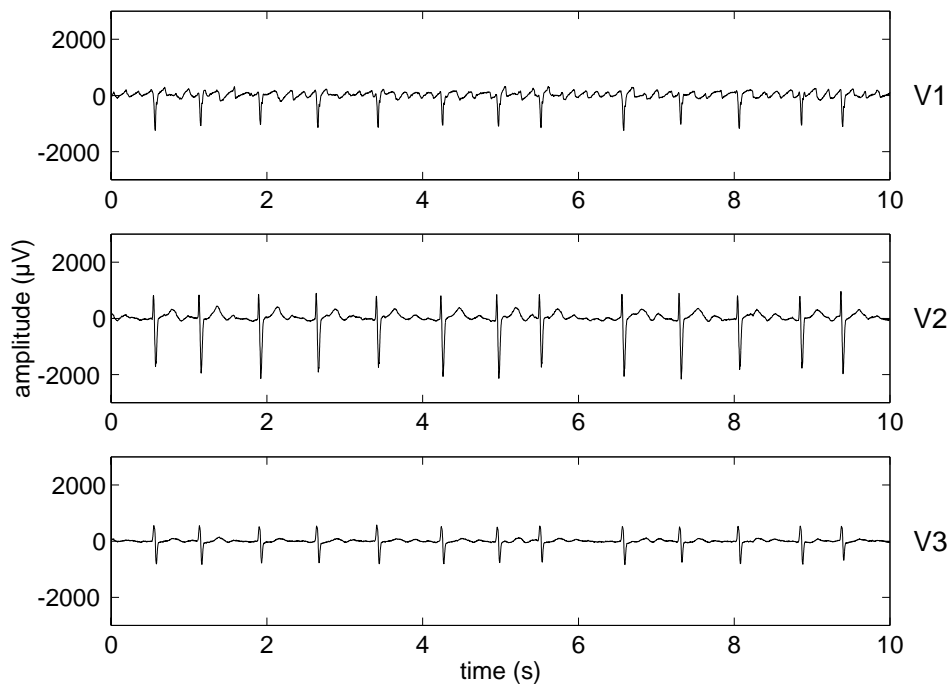
Figure 6: Example of an ECG with atrial fibrillation

to remove the fibrillatory waveforms before the estimation of $\mathbf{Q}$, $\mathbf{D}$ and τ is done. This approach is obviously a contradiction: to get an estimate of $\mathbf{F}$ it must already be known. Our solution to this dilemma is to use a "quick-and-dirty" method to produce an AF estimate to be subtracted from $\mathbf{Y}$ prior to QRST cancellation. A method is used which "fills in" the AF waveforms in the QRS interval by interpolation based on the AF activity contained in the adjacent T-Q intervals; for further details see [5].

5.2 Example on QRST cancellation

The performance of the spatiotemporal QRST cancellation method ("QD alignment") is illustrated with an ECG recording from leads V_1 - V_3, see Fig. 6. The residual ECGs were computed using the ABS and the QD alignment method, see Fig. 7. It is obvious from Fig. 7 that the QRS-related residuals are much better canceled with the QD alignment technique. In this case the improvement is most striking in the leads with weaker AF, i.e. V_2 and V_3. In Fig. 7 (a), the periodically alternating polarity of the QRS-related residuals in lead V_2 of the ABS method suggests that these errors are caused by respiratory-induced variations in QRS complex morphology; these changes are efficiently handled by the QD method, cf. Fig. 7 (b).

16
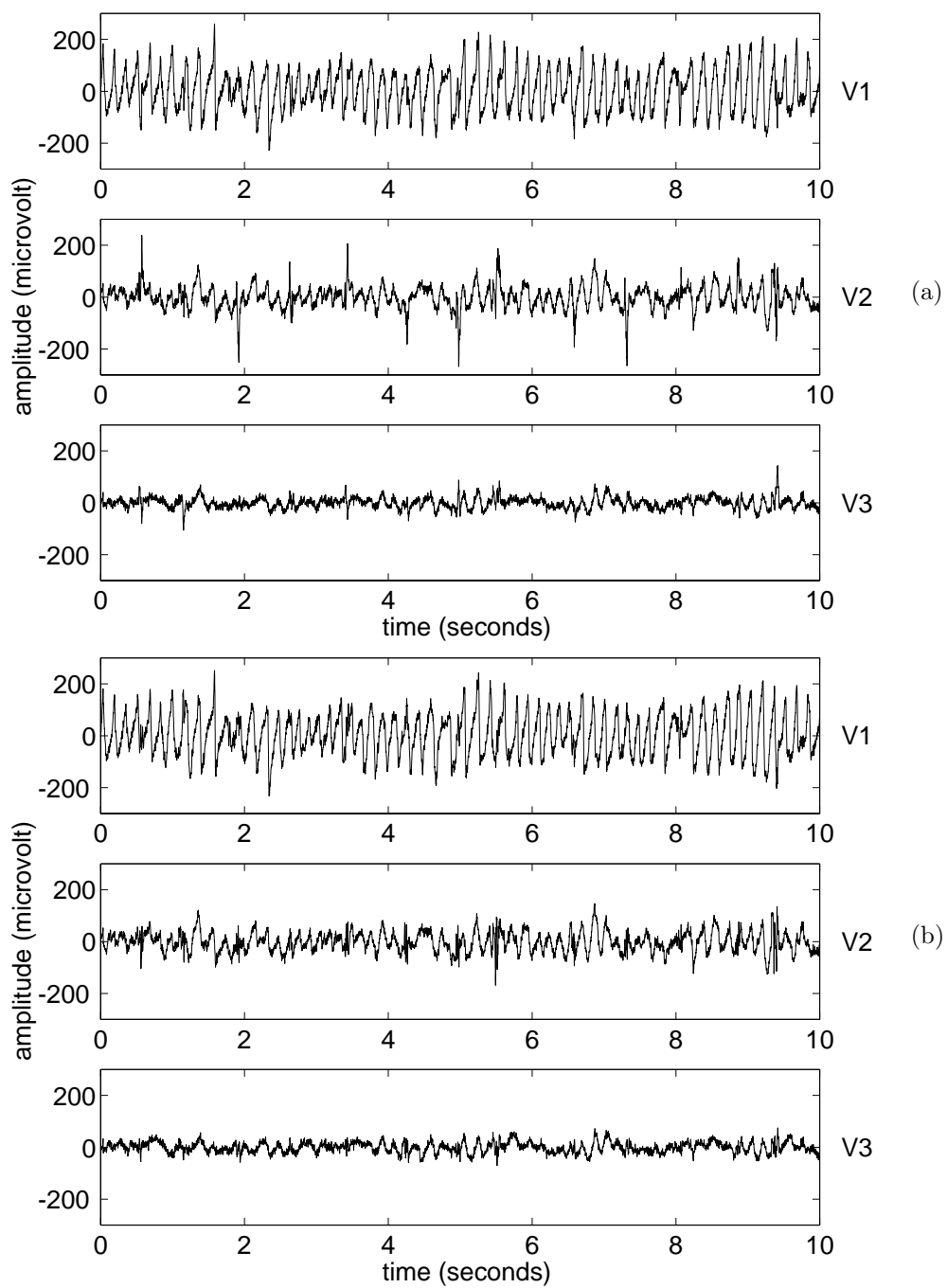
Figure 7: QRST cancellation of the ECG signal shown in Fig. 6 using (a) average
beat subtraction and (b) spatiotemporal alignment.

17

6 Conclusions

The problem of VCG loop alignment has been revisited by means of developing a statistical signal model to which ML estimation was applied. The resulting nonlinear estimation method is feasible from an implementational point of view while it still ensures that the optimal alignment parameter values (scaling, rotation and synchronization) are always found.

The loop alignment was applied to the analysis of subtle beat-to-beat variability in QRS morphology where the cancellation of respiratory-induced variations is important for accurate morphologic measurements. Two examples illustrated that the effects of respiration on morphologic variability can be dramatically reduced by the new technique. Another application is found in the analysis of atrial fibrillation in the surface ECG where QRST cancellation is required. The residual ECG produced by the present alignment method is better suited for e.g. time–frequency AF analysis than that of the ABS method because of the smaller QRS related residuals.

References

[1] J. Fayn, P. Rubel, P. Arnaud, C. Flaemens, M. Frachon, and S. Hacker, "New serial VCG comparison technqiues. Application to the detection of myocardial infarction after bypass surgery," in *Proc. Computers in Cardiology*, pp. 533–536, IEEE Computer Society, 1986.

[2] J. Fayn, P. Rubel, and N. Mohsen, "An improved method for the precise measurement of serial ECG changes in QRS duration and QT interval," *J. Electrocardiology*, vol. 24 (Suppl.), pp. 123–127, 1989.

[3] L. Sörnmo, "Vectorcardiographic loop alignment and morphologic beat-to-beat variability," *IEEE Trans. Biomed. Eng.*, vol. 45, pp. 1401–1413, 1998.

[4] M. Åström, E. Carro, L. Sörnmo, B. Wohlfart, and P. Laguna, "Vectorcardiographic loop alignment, morphologic beat-to-beat variability and the presence of noise," *IEEE Trans. Biomed. Eng.*, Accepted for publ. IEEE Trans. Biomed. Eng.

[5] M. Stridh and L. Sörnmo, "Spatiotemporal QRST cancellation techniques in the surface ECG for improved characterization of atrial fibrillation," in *Proc. of IEEE Eng. Med. Biol. Soc.*, (CD-ROM), 1997.

[6] C. W. Therrien, *Discrete random signals and statistical signal processing.* Prentice-Hall, 1992.

[7] G. Golub and C. van Loan, *Matrix Computations.* The Johns Hopkins University Press, 2nd ed., 1989.

[8] F. Pinciroli, R. Rossi, and L. Vergani, "Detection of electrical axis variation for the extraction of respiratory information," in *Proc. Computers in Cardiology*, pp. 499–502, IEEE Computer Society Press, 1985.

[9] R. Pallas-Areny and F. C. Riera, "Recovering the respiratory rhythm out of the ECG," *Med. Biol. Eng. Comput.*, vol. 23, pp. 338–339, 1985.

[10] S. Ben-Haim, A. Gil, Y. Edoute, M. Kochanovski, O. Azaira, E. Kaplinsky, and Y. Palti, "Beat to beat variation in healed myocardial infarction," *Am. J. Cardiol.*, vol. 68, pp. 725–728, 1991.

[11] J. Nowak, I. Hagerman, M. Ylén, O. Nyquist, and C. Sylvén, "Electrocardiogram signal variance analysis in the diagnosis of coronary artery disease - A comparision with exercise stress test in an angiographically documented high prevalence population," *Clin Cardiol*, vol. 16, pp. 671–682, 1993.

[12] H. Kestler, M. Hoeher, G. Palm, M. Kochs, and V. Hombach, "Time domain variability of high resolution beat-to-beat recordings classified by neural networks," in *Proc. Computers in Cardiology*, pp. 317–320, IEEE Computer Society, 1996.

[13] K. Prasad and M. Gupta, "Phase-invariant signature algorithm. A noninvasive technique for early detection and quantification of Ouabain-induced cardiac disorders," *Angiology*, vol. 30, pp. 721–732, 1979.

[14] J. Malmivuo and R. Plonsey, *Bioelectromagnetism*. Oxford: Oxford University Press, 1995.

[15] L. Sörnmo, B. Wohlfart, J. Berg, and O. Pahlm, "Beat-to-beat qrs variability in the 12-lead ecg and the detection of coronary artery disease," *J. of Electrocardiol.*, vol. 31, pp. 336–344, 1998.

[16] L. Edenbrandt and O. Pahlm, "Vectorcardiogram synthesized from a 12-lead ECG: superiority of the inverse Dower matrix," *J. Electrocardiol.*, vol. 21, pp. 361–367, 1988.

[17] P. MacFarlane, L. Edenbrandt, and O. Pahlm, *12-lead vectorcardiography*. Oxford: Butterworth-Heinemann, 1994.

[18] J. Slocum, E. Byrom, L. McCarthy, A. Sahakian, and S. Swiryn, "Computer detection of atrioventricular dissociation from surface electrocardiograms during wide QRS complex tachycardia," *Circ.*, vol. 72, pp. 1028–1036, 1985.

[19] M. Holm, S. Pehrsson, M. Ingemansson, L. Sörnmo, R. Johansson, L. Sandhall, M. Sunemark, B. Smideberg, C. Olsson, and B. Olsson, "Non-invasive assessment of atrial refractoriness during atrial fibrillation in man - introducing, validating and illustrating a new ECG method," *Cardiovascular Research*, vol. 38, pp. 69–81, 1998.

[20] S. Shkurovich, A. Sahakian, and S. Swiryn, "Detection of atrial activity from high-voltage leads of implantable ventricular defibrillators using a cancellation technique," *IEEE Trans. Biomed. Eng.*, vol. 45, pp. 229–234, 1998.

[21] M. Koschat and D. Swayne, "A weighted Procrustes criterion," *Psychometrica*, no. 2, pp. 229–239, 1991.